Silicon (2021) 13:2221–2232
https://doi.org/10.1007/s12633-020-00733-6

ORIGINAL PAPER

Influence of Ferrotitanium and Silicon Carbide Addition on Structural Modification, Nanohardness and Corrosion Behaviour of Stir-Cast Aluminium Matrix Composites

Samuel Olukayode Akinwamide[1] · Ojo Jeremiah Akinribide[1] · Peter Apata Olubambi[1]

Received: 29 April 2020 / Accepted: 23 September 2020 / Published online: 2 October 2020

Abstract
The use of aluminium based composite is becoming widespread in the industries where enhanced mechanical and improved corrosion resistance properties are required. Microstructural analysis, hardness and corrosion properties of aluminium based composites reinforced with particles of silicon carbide (SiC) and ferrotitanium (TiFe) were investigated. The composites were produced using stir casting technique, with the dispersion of different weight percentages of single and dual reinforced particles within the aluminium matrix. The microstructural evolution, microhardness and nanohardness properties of the as-cast specimens were investigated. Electrochemical testing of specimens was carried out using potentiodynamic polarization and potentiostatic techniques in 3.5 wt.% sodium chloride (NaCl) solution. The microstructural examinations conducted showed a homogeneous dispersion of the SiC and TiFe reinforcements within the aluminium matrix. The hardness (micro and nano) properties of the reinforced specimens were enhanced due factors which include effective load transfer mechanism between the reinforcements and matrix, and an impediment to dislocation movement within the composite. The specimens reinforced with particles of 5% SiC +2% TiFe and 5% SiC exhibited the most improved corrosion resistance from the potentiodynamic polarization and potentiostatic tests conducted. This was confirmed by the surface analysis of corroded specimens carried out using a field emission scanning electron microscope (FE-SEM). The formation of filiform structure on the surface of the unreinforced aluminium alloy and several pits on the surface of the composites was attributed to the aggressive effect of the chloride ions present in the test electrolyte.

Keywords Aluminium matrix composite · Ferrotitanium · Silicon carbide · Potentioststic · Potentiodynamic polarization · Nanohardness

1 Introduction

Progressive research in the field of composite materials development is required to match up with increasing demands for properties such as low density, high strength, high hardness, and improved corrosion resistance in the modern industries [1]. Aluminium based composites that possess properties such as high strength, excellent thermal conductivity, and good damping is suitable for the fabrication of engineering parts like bicycle frames, automobile drive shaft, cylinder block, automotive pistons [2, 3].

Several fabricating techniques have been employed for the development of metal matrix composites. The stir casting technique has found extensive usage due to its cost-effectiveness and simplicity, which makes it appropriate for production in large quantities [4, 5]. In comparison with other fabricating techniques such as additive manufacturing, powder metallurgy, and compocasting. Stir casting is known for promoting excellent bonding between the reinforcement particles and the matrix, thereby leading to improved mechanical and corrosion properties of fabricated composites [6]. To achieve a homogeneous dispersion of the reinforcement particles within the aluminium matrix, the wettability between the aluminium and reinforcement particles must be adequately optimized [7]. This can further enhance the use of these composites for various applications in the engineering sector.

✉ Samuel Olukayode Akinwamide
akinwamidekayode@gmail.com

[1] Centre for Nanomechanics and Tribocorrosion, School of Mining, Metallurgy and Chemical Engineering, University of Johannesburg, Johannesburg, South Africa

Silicon carbide remains one of the most commonly used reinforcements in the fabrication of aluminium based composites [8], due to its suitability for applications where low strength to weight ratio and improved tribological properties are required [9, 10]. The addition of magnesium during casting is also essential as it helps promote wettability between the matrix and reinforcement particles, which results in excellent bonding between the particles [11]. Ferrotitanium, which is produced from low-grade titanium ingots through reduction or melting process is used as additives for producing flux-cored wire as well as the production of military aircraft and stainless steel processing units due to their improved corrosion and mechanical properties [12]. Ferrotitanium which is highly reactive with elements such as oxygen, carbon, and nitrogen has improved features, which include enhanced strength, low density, and improved corrosion resistance [13]. The mechanical properties of silicon carbide particles include thermal shock resistance, high-temperature strength, and excellent wear resistance [14].

The corrosion and hardness properties, among other engineering properties of silicon carbide and ferrotitanium reinforced aluminium based composites fabricated by casting technique, have been reported by different authors [15, 16]. These researchers stated that aluminium based composites are susceptible to pitting corrosion in NaCl electrolyte due to the initiation of pits at secondary phases present in the composite. Rodriguez [17] described the formation of an interface between the aluminium matrix and reinforcement particles as the weakest site in a composite. This, however, indicates that the strength of the interfacial bond is essential in determining the corrosion resistance of the composite.

Alaneme et al. [18] also reported on the microstructural and mechanical behaviour of aluminium matrix reinforced with silicon carbide and rice husk ash particles. The hardness and tensile properties of fabricated composites were improved upon the addition of silicon carbide particles. However, the fracture toughness of the composites was reportedly improved with increased content of groundnut shell ash. A study on the corrosion and mechanical behaviour of silicon carbide and titanium carbide reinforced aluminium matrix composites fabricated by stir casting technique was investigated by Sambathkumar et al. [19].. The corrosion testing of specimen performed in 3.5 wt.% NaCl showed that the corrosion resistance of the composites was enhanced with an increase in volume percentage of silicon carbide and titanium nitride reinforcements. The hardness and tensile properties of the composites, when compared with the unreinforced aluminium alloy, were also reported to be improved.

Recent studies have shown that incorporation of a higher proportion of silicon carbide reinforcement into the matrix of aluminium would result in reduced mechanical properties of the resulting composite through the formation of brittle aluminium carbide (Al_4C_3) phase, thereby limiting its application in the engineering industries [20, 21]. Due to the little existing literature on the microhardness, nanohardness and corrosion studies of stir cast aluminium based composites reinforced with particles of ferrotitanium and silicon carbide, this present research is aimed at investigating the microhardness and nanohardness properties of stir cast ferrotitanium and silicon carbide aluminium matrix composites, and their corrosion resistance in 3.5 wt% NaCl solution.

2 Materials and Method

2.1 Materials

Ingot of commercially pure aluminium (1000X series) supplied by Insimbi alloys South Africa was used as the matrix. At the same time, ferrotitanium (APS: 176 μm) and silicon carbide (APS: 7 μm) powders supplied by industrial analytical were used as reinforcements. The chemical composition of the aluminium ingot and starting powders are shown in Tables 1 and 2 respectively. Figure 1 presents the morphology of the reinforcement particles as analysed with SEM. Figure 1a shows irregular and pointed-edged particles of SiC particles. A remarkable characteristic of SiC crystal structure is the polytypic structure it exhibits, and this accounts for variation in stoichiometric ordering in the arrangement of silicon and carbon atoms [22]. The particles of ferrotitanium which exhibits a rocky shaped as seen in Fig. 1b has been reported in a study by Shah et al. [23] to contain a β-Ti, α-Ti and FeTi phases, with β-Ti phase bring thermodynamically unstable at ambient temperature. The presence of other non-equilibrium phases may also exist in the particles due to varying processing conditions.

2.2 Method

2.2.1 Fabrication of Specimens

An electrical resistance furnace was used for melting the as-received aluminium ingot at a temperature of 720 °C. Ferrotitanium and silicon carbide powders were preheated at a temperature of 300 °C in a muffle furnace to eliminate any moisture present in the powders. The preheated powders and 1 g of magnesium were added to the melt of aluminium and manual stirred for 10 mins to ensure proper dispersion of the reinforcement particles in the aluminium matrix. Magnesium

Table 1 Elemental composition of as-received aluminium alloy

Element	Si	Fe	Cu	Mn	Mg	Al
% Composition	0.15	0.34	0.05	0.01	0.06	Balance

Table 2 Elemental composition of silicon carbide powder and ferrotitanium powders

Elements	Al	Fe	Ba	Mn	Ca	K	Mg	Cr	Ni	Si	Ti
SiC	0.21	0.23	0.05	–	0.04	0.04	0.01	–	0.01	99.21	0.02
TiFe	0.36	56.55	–	0.07	0.03	–	0.09	0.03	0.11	0.56	41.67

was added to the melt to improve the wettability between particles of the matrix and reinforcements. To ensure fluidity of the molten metal, the die mould was preheated for 2 h. The pictorial representation of the as-cast specimens and the dimension of the die mould are shown in Fig. 2a and b respectively.

2.2.2 Evaluation of Microstructural and Hardness Properties

The specimens for microstructural examination were prepared using standard metallography procedures, after which they were examined on a ZEISS SIGMA VP Field Emission Scanning Electron Microscope. The phase analysis was investigated using a PW 1710 Philips diffractometer, which is equipped with a monochromatic Cu-Kα radiation at 20 mA and 40 kV. The hardness property of the specimens was determined using a Falcon 500 microhardness tester. A load of 100 g with a dwell time of 10 s was maintained throughout the test. A total of five points were indented across the matrix and reinforcement phases as shown by the microscope attached to the hardness tester, and the hardness value of each specimen was obtained from the average values from each indent. Nanohardness testing of specimens was performed on a UNHT3 HTV Anton Paar Ultra nanoindenter, equipped with a high precision Berkovich diamond indenter. A load of 50 mN was applied at a loading and unloading rate of 60 mN/min, while the contact force and acquisition rate were maintained at 10 mN and 10 Hz, respectively. The nanohardness value of each specimen was obtained from the average of the values recorded from 10 indentations, at a spacing of 8 μm. Adequate spacing is essential to prevent work hardening on the specimen surface [24]. The microhardness and nanohardness testing of the specimens were carried out in accordance with ASTM E-92 and ISO 14577-1 standards, respectively. The micro and nanohardness tests were conducted due to the slight variation observed between the nanohardness and microhardness values recorded by the specimens. During nanoindentation measurements, indents are made at the centre of the grains, and the nanohardness value is evaluated from the maximum area of indent, and maximum force applied [25]. Conversely, the indented area on the specimen is only considered after indentation during microhardness measurement.

2.2.3 Corrosion Testing

Electrochemical measurements were carried using potentiostatic and potentiodynamic polarization techniques according to ASTM 94, using a Versastudio software on VersaSTAT 4 electrochemical testing machine. This equipment is equipped with a conventional three-electrode system consisting of reference, counter, and working electrode probes. The specimens used as working electrodes were prepared by attaching a copper wire to one end of the sectioned samples, after which they were cold mounted in epoxy resin. The surface was prepared for the corrosion test by grinding the surface of the specimen to 800 silicon carbide paper and polishing with 6 μm suspension on an Aka Daran disc. A graphite rod and silver/silver chloride (Ag/AgCl) electrode were used as the counter and reference electrodes, respectively. Potentiodynamic polarization measurement was carried out at a scan rate of 0.2 mV/s starting from −1 V to 0.5 V. In contrast, potentiostatic tests were carried out for 2 h, using the value of corrosion potential from each specimen. A time

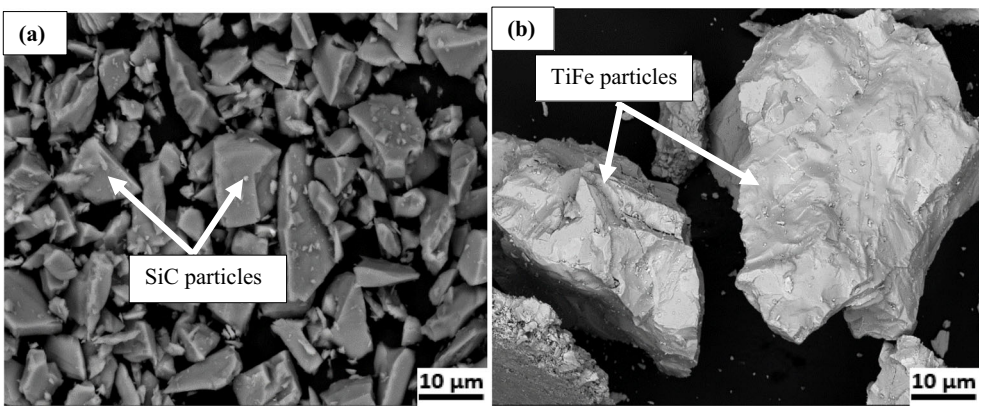

Fig. 1 SEM morphology of (**a**) silicon carbide and (**b**) ferrotitanium reinforcement particles

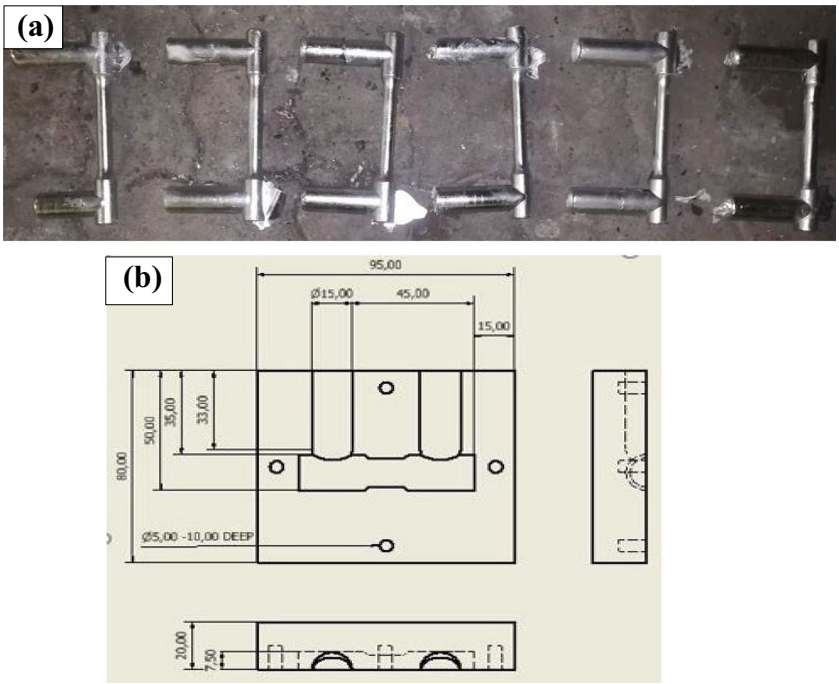

Fig. 2 **a** Images of fabricated specimens (**b**) engineering drawing of die mould used for casting

per point of 0.5 was used for all the specimens. Electrolytes were replaced after each scan, and tests were repeated three times for reproducibility purposes. The corrosion rate of the specimens was calculated according to Eq. 1 [26]. The surface of the test specimens was examined using an FE-SEM to determine the nature of pits formed after the corrosion tests.

$$C_R = \frac{0.00327 \times Corr_i \times E_w}{\delta} \quad (1)$$

Where C_R = Corrosion rate (mm/yr), 0.00327 = Corrosion rate constant, $Corr_i$ = Corrosion current density, E_w = Equivalent weight, δ = Density.

3 Results and Discussion

3.1 Microstructural Characterization and Phase Analysis of as-Cast Specimens

Figure 3a shows the SEM analysis of the as-cast aluminium alloy and composites reinforced with varying proportions of SiC and TiFe reinforcements. The presence of silicon particles, which is the major alloying element of the as-cast aluminium alloy is visible across the micrograph shown in Fig.3a. Furthermore, Fig. 3b and c reveal the homogeneous distribution of single particles of SiC and TiFe reinforcements within the aluminium matrix. The even dispersion observed can however, be ascribed to the adequate frictional force generated between the reinforcements and aluminium particles during stirring [27]. A similar observation was also reported in a study by Lin et al. [28] . Figure 3d and e shows the distribution 2% SiC +2% TiFe and 5% SiC and 5% TiFe reinforcements in the aluminium alloy matrix. The clustering of the reinforcement particles, as seen in the micrographs, represents a clear interface between the aluminium matrix and reinforcements [29]. It should be further noted that the enhanced wettability between the reinforcement particles and aluminium matrix would improve the interfacial bond strength of the resulting composites [30, 31].

The XRD analysis of the binary and ternary reinforced composite systems is presented in Fig. 4a and b, respectively. The miller indices at which different peaks are formed due to the dispersion of SiC and TiFe particles within the aluminium matrix as identified by the analysis carried out on X'pert Highscore software is given as (110), (200), (220), (311) and (222). The software further reveals that the atomic arrangement of the composite is represented as a hexagonal closed packed system. Some of the phases formed in the binary composite system (Fig. 4a) include AlTi, Al_9Si, $Al_{0.5}Fe_3Si_{0.5}$ and Al_2FeSi, while the phases of Al_3SiO_{47}, $Al_8Si_6Mg_3Fe$, and $Fe_{17}.Al_4Si$ are dominant in the ternary system composites (Fig. 4b). However, it noteworthy that the cubic arrangement of the formed phases is sufficient to confirm the polycrystalline structure of the composites. A similar observation was reported in a recent study by Albiter et al. [32]

3.2 Hardness Properties of Aluminium Alloy and Composites

The microhardness values obtained for the fabricated aluminium alloy and composites are presented in Fig. 5. The highest hardness value of 35.8 HV was seen in the specimen with

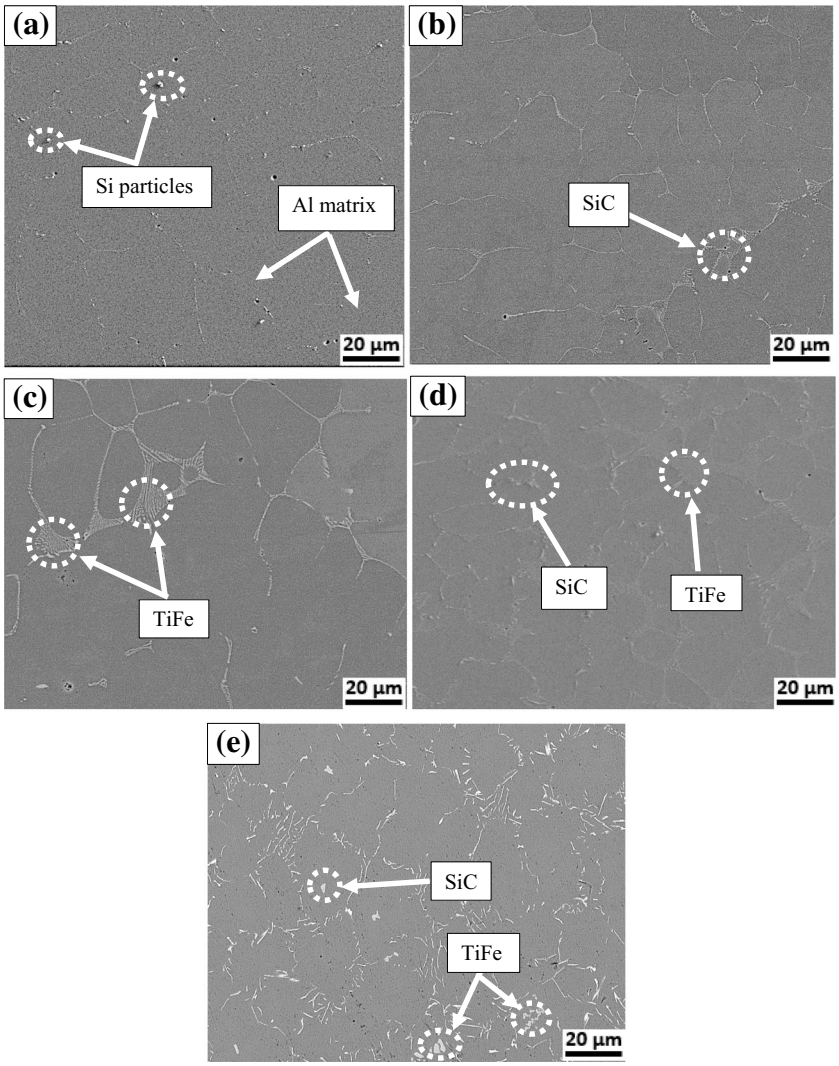

Fig. 3 SEM examination of (**a**) Al alloy (**b**) Al + 2% SiC (**c**) Al + 2% TiFe (**d**) Al + 2% SiC +2% TiFe (**e**) Al + 5% SiC +5% TiFe

5 wt.% SiC reinforcement, while as-cast aluminium alloy recorded the lowest value of 25 HV. The improvement in hardness observed in reinforced specimens can be ascribed to microstructural refinement caused by the incorporation of reinforcement particles into the aluminium alloy matrix. The homogeneous dispersion of TiFe and SiC particles within

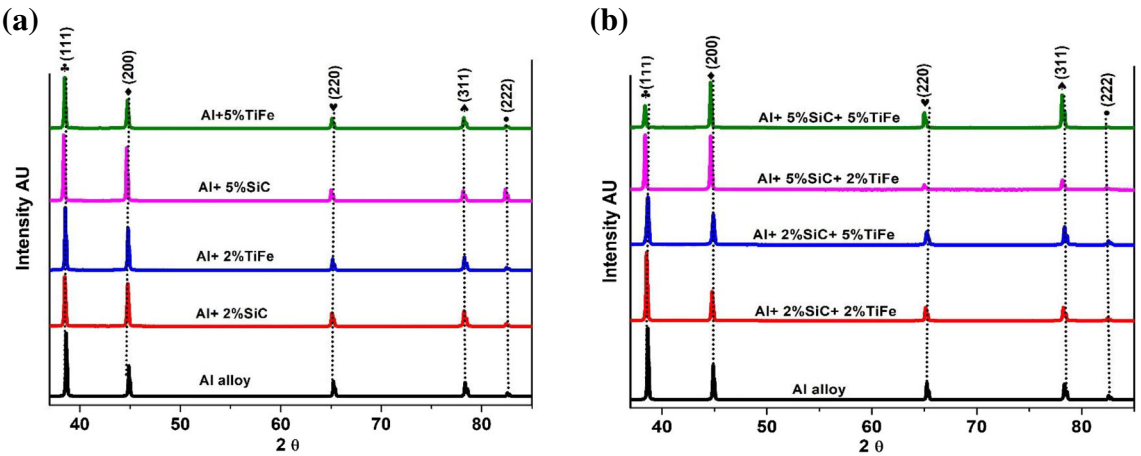

Fig. 4 Phase analysis of as-cast aluminium alloy and composites

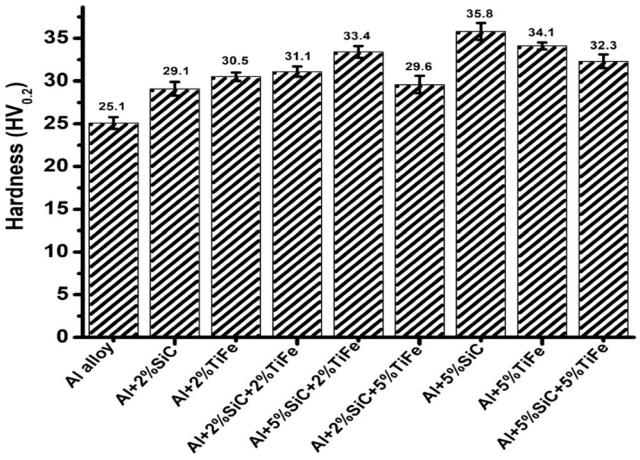

Fig. 5 Hardness plot for fabricated aluminium composite systems

the matrix hinders the movement of dislocation, thereby disrupting the dislocation paths as they continue to bend and enclose the particles present in the matrix completely before the dislocation motion continues. This process is referred to as the Orowan strengthening mechanism [33]. However, the presence of the enclosed particles leads to increased dislocation density of composites when compared to the as-cast aluminium alloy. Moreover, the formation of extra dislocations within the composite can be as a result of differential deformation and thermal mismatch between the reinforcement particles and aluminium alloy matrix. A similar observation was reported in an investigation by Casati and Vedani [34]. Strengthening by the coefficient of thermal expansion mismatch is caused by the formation of dislocation accommodated by the mismatch between the matrix and reinforcement particles during cooling. The coefficient of thermal expansion can, therefore, be calculated using Eq. 2.

$$\Delta\sigma_{CTE} = B\mathrm{M}_s b\sqrt{D^{CTE}} \tag{2}$$

Where B = 1.25, M_s = shear modulus of matrix, b = Burgers dislocation vector and D^{CTE} = dislocation density.

However, Ms. and D^{CTE} can be calculated using Eqs. 3 and 4.

$$M_s = \frac{E_y}{2(1+V)} \tag{3}$$

and

$$\frac{D^{CTE} = a\Delta\alpha\Delta T V_p}{b d_p(1-V_p)} \tag{4}$$

Where E_y = young modulus, V = Poisson's ratio, $\Delta\alpha$ = difference in coefficient of thermal expansion between matrix and reinforcements, 'a' = constant value of 12, ΔT = difference between room and pouring temperature, V_p = volume fraction and d_p = average particle size.

Furthermore, the thermal contraction difference between reinforcement particles and aluminium matrix can result in a hardening effect [27, 35]. The Hall-Petch relationship describes the hardness property of aluminium based composites based on grain size effect [36]. The grain size of fabricated composites is, however, smaller compared to that of aluminium alloy matrix as a result of the refinement of reinforcement grain particles. This leads to an appreciable increase in the hardness property of the fabricated composites. The relationship between the average grain size of composites and Hall Petch coefficient is represented by Eq. 5.

$$\Delta\sigma_{HP} = K\Delta\left(G^{-0.5}\right) \tag{5}$$

Where K = Hall-Petch Coefficient and G = average grain size.

Further, an increase in weight percentage of SiC and TiFe reinforcements can reduce the inter-particle distance within the composite, thereby resulting in an increase in the stress required for dislocation movement between the particles [37, 38]. The dispersion of both SiC and TiFe reinforcements in varying proportions within the aluminium matrix is also seen to improve the hardness property of the resulting composites. However, a decrease in hardness value was further observed in composites reinforced with a higher proportion of SiC (5% SiC +2% TiFe and 5% SiC +5% TiFe) due to the formation of brittle intermetallic phases which resulted from the interaction between the reinforcement and the aluminium matrix particles [39, 40]. Most of the loads are therefore assumed to be borne by the interphase formed between the aluminium alloy matrix and the TiFe reinforcement particles. The hardness values of fabricated aluminium alloy and composites are also presented in Table 3.

Figure 6 shows the plot of nanohardness values for the as-cast specimens. The nanohardness property of all reinforced composites is observed to be enhanced when compared with the unreinforced aluminium alloy. The composite reinforced with 5% SiC recorded a nanohardness value of 1458 MPa, while the least value of 460 MPa was recorded by the unreinforced aluminium specimen. The improved nanohardness properties evident in the reinforced composites can be as a result of an impediment to both dislocation movement and plastic deformation within the composites due to the presence of SiC and TiFe reinforcement particles [13, 41]. Further, the outstanding nanohardness value observed in the composite reinforced with 5% SiC reinforcement can be attributed to the formation of secondary carbide phase (aluminium carbide) due to the interaction between the aluminium and silicon carbide. This carbide helps in improving the mechanical properties of composites.

Table 3 Corrosion rate and Tafel properties of specimens in NaCl electrolyte

Specimen	Corrosion current density (μA)	Corrosion potential (V)	Cathodic slope, Bc (V/Dec)	Anodic slope, Ba (V/Dec)	Corrosion rate (mm/yr)
Al	289.15	−1.05	0.23	0.23	3.15
Al + 2%SiC	5.83	−0.68	0.31	0.31	0.06
Al + 2%TiFe	208.34	−1.01	0.24	0.24	2.27
Al + 2%SiC+2%TiFe	87.45	−0.98	0.18	0.18	0.95
Al + 2%SiC+5%TiFe	0.51	−0.23	0.19	0.11	0.01
Al + 5%SiC+2%TiFe	1.93	−0.39	0.042	0.34	0.02
Al + 5%TiFe	75.13	−0.92	0.34	0.34	0.82
Al + 5%SiC	3.28	−0.66	0	0.58	0.41
Al + 5%SiC+5%TiFe	405.45	−1.07	0.23	0.23	4.42

3.3 Potentiodynamic Polarization

Figure 7 shows the polarization plots for single-particle reinforced aluminium composites in 3.5 wt.% NaCl, with all the curves showing similar passivation characteristics and polarization trend. Further observations show that the presence of chloride ions in the electrolyte dissolves the passive layers formed on the specimen surface, thereby resulting in the anodic dissolution of the composites. The highest corrosion rate of 3.15 mm/yr recorded by the unreinforced aluminium alloy can be as a result of the galvanic coupling between the alloying elements and the aluminium matrix, leading to the rapid dissolution of the alloy in the electrolyte, accompanied by a positive shift in current density. However, improved corrosion resistance observed in the specimen with 5% SiC reinforcement (corrosion rate of 0.41 mm/yr) can be attributed to the anodic inhibition effect of SiC particles. The negative shift in potential values of −0.68 V and − 0.92 V seen in composites reinforced with 2% SiC and 5% TiFe particles respectively, shows the cathodic inhibition of hydrogen evolution and oxygen reduction at the surface of Al/SiC and Al/TiFe interfaces [42]. This improved corrosion resistance observed in the reinforced composites can also be attributed to the formation of chloride oxide complexes formed on the surface of the composites, due to oxygen reduction. Moreover, the passivation behaviour observed in all specimens is also a confirmation of chloride ions complexes, which leads to a break down of formed oxide films after the displacement of oxygen from the transpassive region of the curve [43].

Aluminium alloys are known for their ability to resist corrosion attack in aggressive environments, due to their ability to form protective oxide layers. These oxide films act as a kinetic barrier that prevents the oxidation of the underlying reactive metal in a process called passivation. The formed passive film becomes unstable and degrades locally in the chloride environment, resulting in rupturing of films and localized corrosion. This form of corrosion occurs according to the following mechanisms in chloride environment: (i) ion

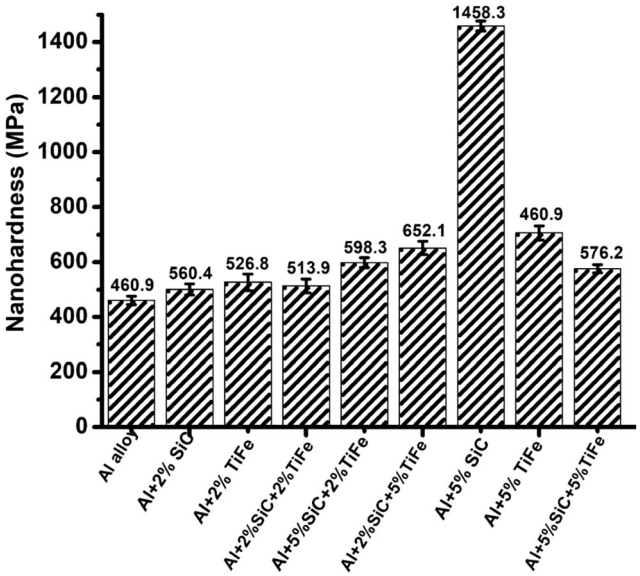

Fig. 6 Nanohardness plot for fabricated aluminium composite systems

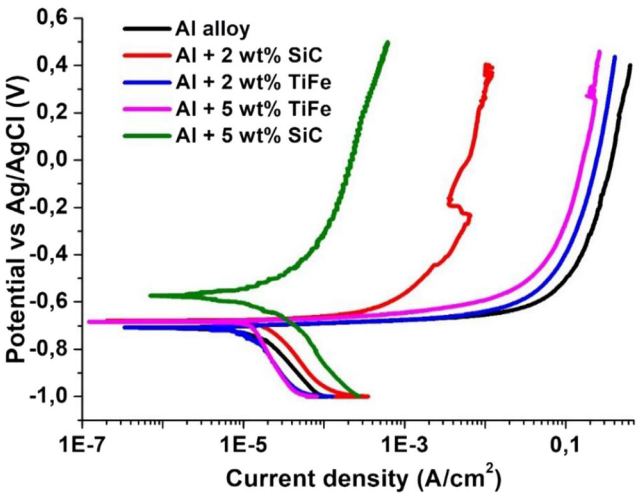

Fig. 7 Potentiodynamic polarization curves for aluminium alloy and single particle reinforced composite

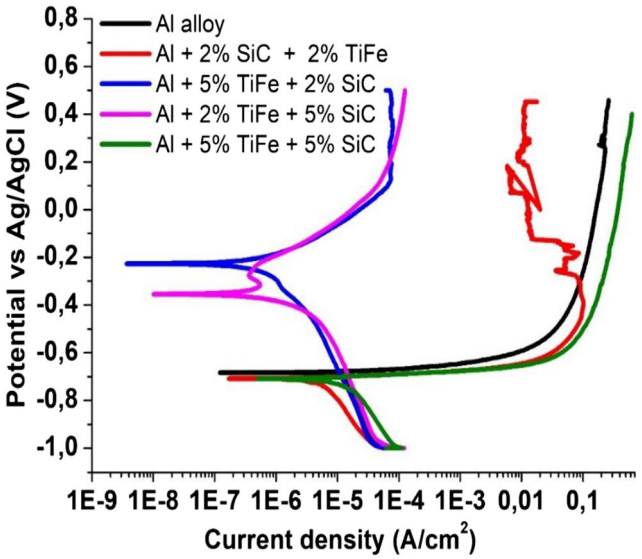

Fig. 8 Potentiodynamic polarization curves for aluminium alloy and dual particle reinforced composite systems

migration/penetration of oxide (ii) displacement of ions resulting in thinning of oxides (iii) rupturing and repair of oxide layers.

The polarization curves for unreinforced aluminium alloy and the dual particle reinforced aluminium composites are presented in Fig. 8. As a result of the corrosive nature of the electrolyte, the deterioration observed on the surface of the specimen with 5% SiC +5% TiFe reinforcement was severe as it records a corrosion rate of 4.42 mm/yr. However, the corrosion potential (Ecorr) values determine the thermodynamic stability and tendency of the reinforced composites to corrode in the aggressive chloride electrolyte. The Ecorr value of −0.23 V recorded by the specimen reinforced with 2% SiC

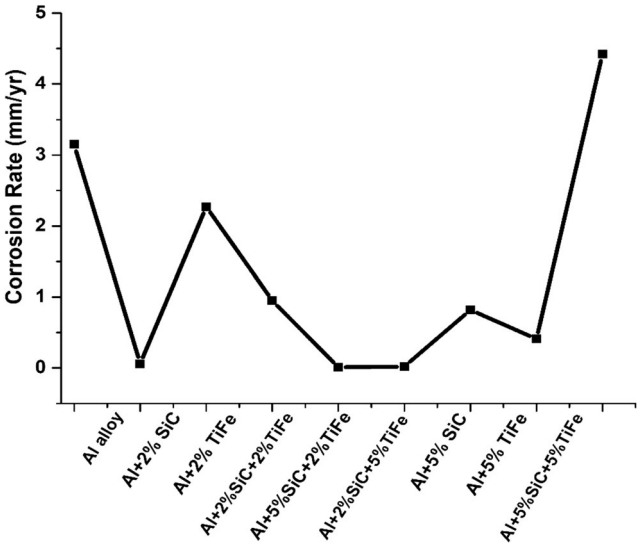

Fig. 9 Plot of corrosion rate for fabricated aluminium alloy and composites

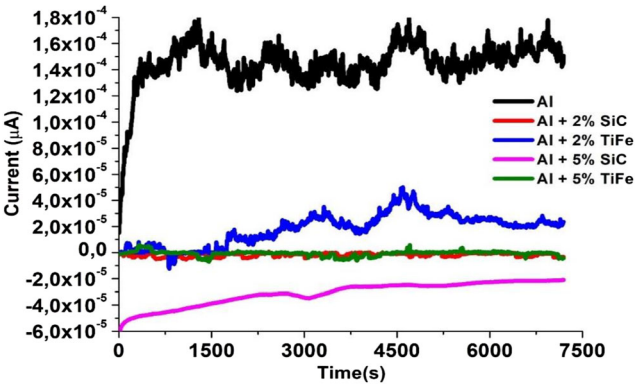

Fig. 10 Potentiostatic curves for single particle reinforced aluminium composite

+5% TiFe particles is observed to be more electronegative due to a reduction in the selective adsorption of the chloride anions on the surface of formed passive oxide layers. The enhanced corrosion resistance exhibited by composites with 2% SiC +5% TiFe reinforcements and 5% SiC +2% TiFe reinforcements further confirms the formation of passive layers across the surface of the specimens, due to the reduction reaction of oxygen atoms [44]. Also, the overall improved corrosion resistance in silicon carbide reinforced composites confirms the effect of SiC particles addition on the corrosion resistance of the aluminium alloy, as this affects the stability of the formed oxide layers in the chloride media. Mayyas et al. [45], however, gave a similar report on the effect of SiC addition on the corrosion behaviour of aluminium matrix composites. The polarization data and the corrosion rates for all specimens are further presented in Table 3. The table illustrates the destructive action of the chloride ions on the aluminium alloy and composites as a result of the synergistic effect which occurred between the matrix and the reinforcements at the interfacial layers during redox electrochemical process [46]. The plot of corrosion rates for the as-cast aluminium alloy and reinforced composites is shown in Fig. 9.

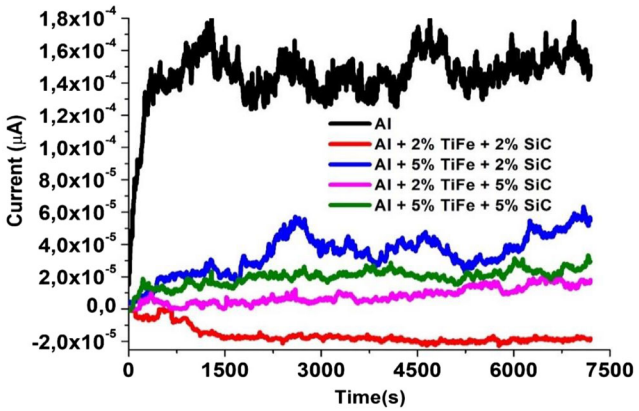

Fig. 11 Potentiostatic curves for aluminium alloy and dual particle reinforced composite systems

3.4 Potentiostatic Polarization

Potentiostatic tests were further conducted on the specimens to have an additional understanding of the corrosion process. This test is carried out by monitoring the change in current at a constant corrosion potential E_{corr}. Potentiostatic tests were conducted for 2 h using the E_{corr} values obtained from open circuit potential tests [47]. Figure 10 shows the potentiostatic curves for unreinforced aluminium alloy and single reinforced aluminium matrix composites. Upon the application of corrosion potential of −0.71 V to the unreinforced aluminium alloy, a sporadic rise in current density from 0 A to 1.4×10^{-4} A is observed, after which steady oscillations were evident till the end of the test. These oscillations can be ascribed to the instability of the passive layer formed on the surface of the specimen. However, minor fluctuations at lower current densities seen in specimens with 5% SiC and 5%TiFe reinforcement shows that the surface of the specimen is adequately coated with passive layers in the electrolyte [48]. The slight increase in current density seen in composite reinforced with 2% TiFe can be ascribed to partial removal of formed oxide layer during the test. The stable curve observed in composite with 2% SiC reinforcement indicates that the occurrence of galvanic coupling between the aluminium matrix and reinforcement is less significant, thereby leading to the improved corrosion resistance of the specimen [49].

Figure 11 shows the plot of current density against time for the dual particle reinforced composite systems. An increase in current density with increasing time was observed in composite reinforced with 2% SiC +5% TiFe particles. Conversely, the steady current density after the first 300 s seen in composites reinforced with 2% SiC +2% TiFe and 5% SiC +5% TiFe

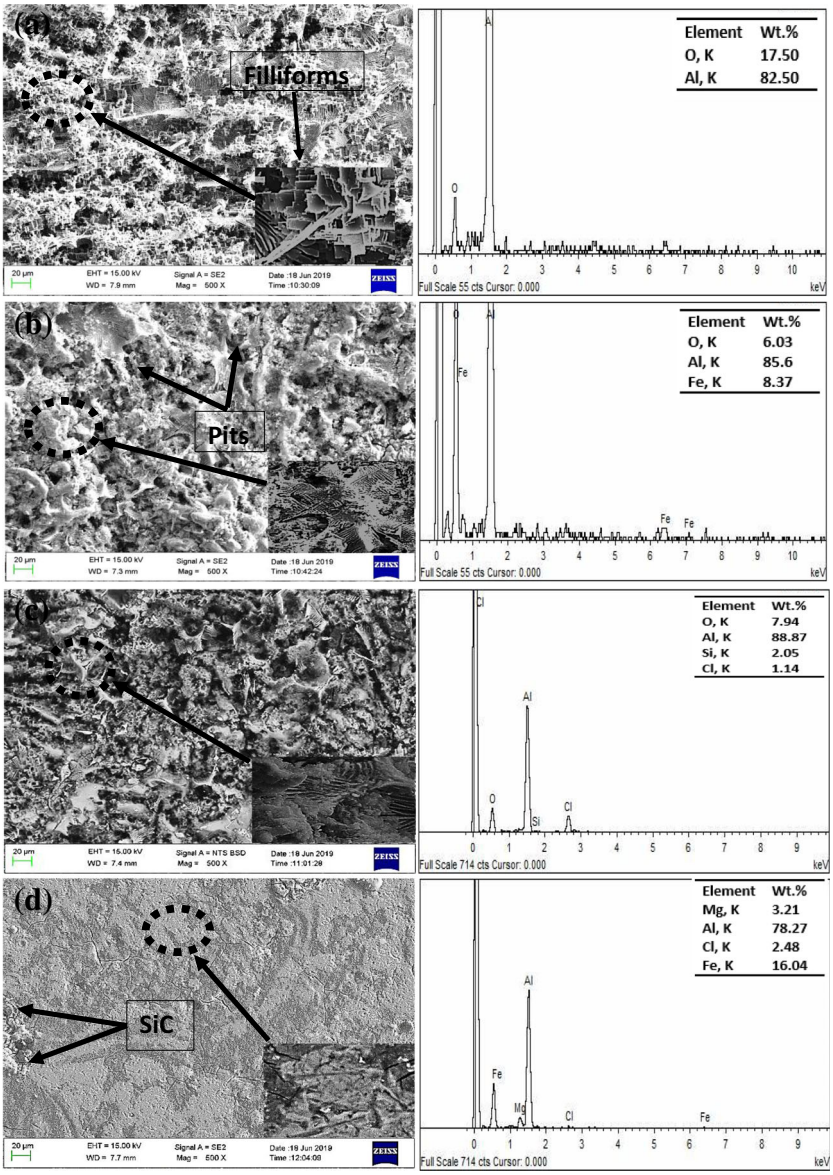

Fig. 12 Surface morphology of (**a**) aluminium alloy (**b**) Al + 2%SiC (**c**) Al + 2%TiFe (**d**) Al + 5%SiC after exposure to corrosive medium

shows the growth of metastable pit initiated on the surface of the specimen [50]. Metastable pits are known to initiate and grow for a while before the material repassivates [51]. However, the current density of composites with 2% SiC +5% TiFe and 5% SiC +2%TiFe reinforcements were seen to be more stabilized from start to the end of the test. This connotes the formation of a passive layer on the specimen surface. The slight increase in fluctuations observed after the first 200 s in composite with 5% of SiC +5% TiFe can further be attributed to the initiation of the oxygen evolution reaction. The current density response is mainly a function of factors such as oxygen evolution process, passive layer formation, and passive layer dissolution.

3.5 Microstructural Analysis of Substrates

Figure 12 shows the SEM morphology of the specimens after the potentiodynamic polarization test in the chloride electrolyte. Figure 12a presents the dissolution of aluminium alloy in the electrolyte with evidence of pit formation on several sites along the grain boundaries. The corrosion reaction, which was initiated at different pitting sites was also observed to spread across the surface of the specimen. The SEM morphology of the corroded surface of the aluminium alloy, it is seen to exhibit a filiform type of corrosion which is often characterized by fine thread-like filaments emerging from several sites in different directions [52]. The distribution of pits across the surface of composite with 2% SiC reinforcement shown in Fig. 12b is observed to be lesser, thereby resulting in a reduced corrosion rate, which could be ascribed to the formation of an intermediate phase between the SiC reinforcement particles and the aluminium matrix [53]. This intermediate phase improves the corrosion resistance of the composite by preventing the formation of more pits across the surface of the composite. Figure 12c presents the deteriorated surface of the composite with 2% TiFe reinforcement, resulting from the weakening effect of the chloride anions present in the test electrolyte, which further causes the discharge of metal ions in the electrolyte. Figure 12d shows the surface of the specimen reinforced with 5% SiC. The improved corrosion resistance seen in this specimen can be ascribed to the lesser formation of pits in areas with defects such as inclusions and pores. These pits are often formed from the chemical interaction and adsorption between the chloride anions present in the electrolyte, and the passive oxide layers formed around the defects [54].

Figure 13a shows that the dispersion of different proportions of SiC and TiFe reinforcements within the matrix of aluminium can reduce the attack of the chloride ions on the surface of the resulting ternary aluminium-based composites. Figure 13b shows the aggressive effect of the chloride ions as they penetrate through the weaker points and breakages present on the formed passive oxide fills, thereby resulting in deterioration of the specimen surface. This is also an indication that excessive distribution of the reinforcement particles within the matrix of the aluminium alloy can lead to rapid deterioration of the resulting composite due to increased galvanic corrosion between the matrix and the reinforcements [55, 56].

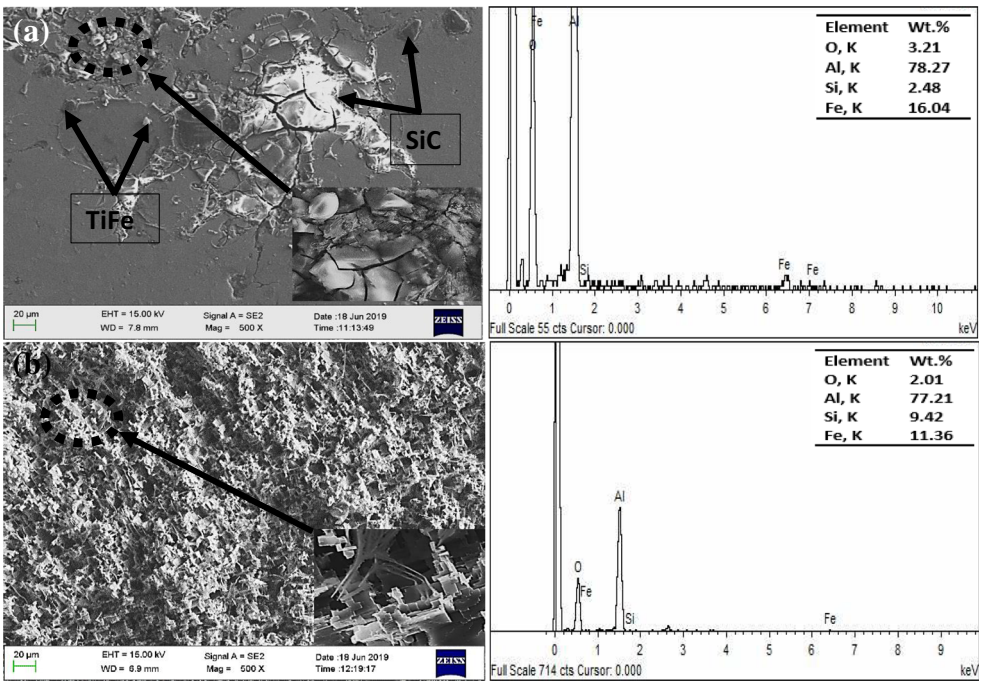

Fig. 13 Surface morphology of (**a**) Al + 2%SiC+2%TiFe (**b**) Al + 5%SiC+5%TiFe composites after exposure to corrosive medium

4 Conclusion

The microstructural properties, hardness (micro and nano), and corrosion properties of SiC and TiFe reinforced aluminium matrix composites fabricated by stir casting technique were investigated. The effectiveness pf the stir casting technique was confirmed in this study as particles of SiC and TiFe reinforcements were confirmed to be homogeneously dispersed within the matrix of aluminium alloy by the SEM and XRD analysis. The improved microhardness recorded in the reinforced composites was ascribed to mechanisms such as Orowan strengthening and thermal expansion coefficient. The nanohardness property of the reinforced composite was also enhanced due to impediment to dislocation movement due to the presence of SiC and TiFe reinforcement particles in the composite. Further, the addition of these reinforcements also increased the rate at which oxide layers are formed on the surface of the composites, thereby improving their corrosion resistance. The least corrosion resistance was seen in the unreinforced aluminium specimen due to its increase in current density in the chloride electrolyte. The SEM analysis of the surface of the specimens after corrosion showed that the corrosion resistance of the specimens reinforced with 5% SiC +2% TiFe and 5% SiC particles respectively was more enhanced.

Acknowledgments The authors are grateful to Global Excellence and Stature of University of Johannesburg and National Research Foundation South Africa for funding.

Compliance with Ethical Standards

Declaration The manuscript is original and no part of it has been published or under consideration for publication somewhere else. There is also no conflict of interest to declare in relation to this research.

References

1. Akinwamide SO, Tshabalala N, Falodun OE, Oke SR, Akinribide OJ, Abe BT et al (2019) Microstructural and corrosion resistance study of sintered Al-tin in sodium chloride solution. Materials Today: Proceedings 18:2881–2886
2. Ahamed AR, Asokan P, Aravindan S, Prakash M (2010) Drilling of hybrid Al-5% SiC p-5% B 4 C p metal matrix composites. Int J Adv Manuf Technol 49:871–877
3. Adams FV, Akinwamide SO, Obadele B, Olubambi PA (2020) Comparison study on the corrosion behavior of aluminum alloys in different acidic media. Proceedings, Materials Today
4. Kalaiselvan K, Murugan N, Parameswaran S (2011) Production and characterization of AA6061–B4C stir cast composite. Mater Des 32:4004–4009
5. Akinribide OJ, Akinwamide SO, Ajibola OO, Obadele BA, Olusunle SO o, Olubambi PA (2019) Corrosion behavior of ductile and austempered ductile cast iron in 0.01 M and 0.05 M NaCl Environments. Procedia Manufacturing 30:167–172
6. Singh MK, Gautam RK (2017) Synthesis of copper metal matrix hybrid composites using stir casting technique and its mechanical, optical and electrical behaviours. Trans Indian Inst Metals 70: 2415–2428
7. Kumar BP, Birru AK (2017) Microstructure and mechanical properties of aluminium metal matrix composites with addition of bamboo leaf ash by stir casting method. Trans Nonferrous Metals Soc China 27:2555–2572
8. Alaneme KK, Bamike BJ (2018) Characterization of mechanical and wear properties of aluminium based composites reinforced with quarry dust and silicon carbide. Ain Shams Engineering Journal 9: 2815–2821
9. Fei T, Kun Y, Jie L, Fang H-j, Shi C-l, Dai Y-l et al (2016) Microstructures and properties of Al–50% SiC composites for electronic packaging applications. Trans Nonferrous Metals Soc China 26:2647–2652
10. Zhang L, Xu H, Wang Z, Li Q, Wu J (2016) Mechanical properties and corrosion behavior of Al/SiC composites. J Alloys Compd 678: 23–30
11. Akinwamide SO, Lemika SM, Obadele BA, Akinribide OJ, Abe BT, Olubambi PA (2019) Characterization and mechanical response of novel Al-(mg–TiFe–SiC) metal matrix composites developed by stir casting technique. J Compos Mater 53:3929–3938
12. Li G, Jin X, Wang D, Chen GZ (2009) Affordable electrolytic ferrotitanium alloys with marine engineering potentials. J Alloys Compd 482:320–327
13. Akinwamide SO, Lemika SM, Obadele BJ, Akinribide OJ, Falodun OE, Olubambi PA, et al. (2019) A nanoindentation study on Al (TiFe-Mg-SiC) composites fabricated via stir casting," in Key Engineering Materials, pp. 81–88
14. Mo R, Yin X, Ye F, Liu X, Ma X, Li Q, Zhang L, Cheng L (2019) Electromagnetic wave absorption and mechanical properties of silicon carbide fibers reinforced silicon nitride matrix composites. J Eur Ceram Soc 39:743–754
15. Kiourtsidis GE, Skolianos SM (2007) Pitting corrosion of artificially aged T6 AA2024/SiCp composites in 3.5 wt.% NaCl aqueous solution. Corros Sci 49:2711–2725
16. Kiourtsidis G, Skolianos SM (1998) Corrosion behavior of squeeze-cast silicon carbide-2024 composites in aerated 3.5 wt.% sodium chloride. Mater Sci Eng A 248:165–172
17. Rodriguez EL (1987) Corrosion of glass fibres. J Mater Sci Lett 6: 718–720
18. Alaneme KK, Bodunrin MO, Awe AA (2018) Microstructure, mechanical and fracture properties of groundnut shell ash and silicon carbide dispersion strengthened aluminium matrix composites. Journal of King Saud University-Engineering Sciences 30:96–103
19. Sambathkumar M, Navaneethakrishnan P, Ponappa K, Sasikumar K (2017) Mechanical and corrosion behavior of Al7075 (hybrid) metal matrix composites by two step stir casting process. Latin american journal of solids and structures 14:243–255
20. Tokariev O, Schnetter L, Beck T, Malzbender J (2013) Grain size effect on the mechanical properties of transparent spinel ceramics. J Eur Ceram Soc 33:749–757
21. Ourdjini A, Chew K, Khoo B (2001) Settling of silicon carbide particles in cast metal matrix composites. J Mater Process Technol 116:72–76
22. Izhevskyi V, Genova L, Bressiani J, Bressiani A (2000) "review article: silicon carbide," *Structure, properties and processing*. Cerâmica 46:4–13
23. Shah SJ, Henein H, Ivey DG (2013) Microstructural characterization of ferrotitanium and ferroniobium. Mater Charact 78:96–107
24. Akinwamide SO, Akinribide OJ, Olubambi PA (2020) Microstructural evolution, mechanical and nanoindentation studies of stir cast binary and ternary aluminium based composites. Journal of Alloys and Compounds, p. 156586

25. Sánchez-Martín R, Pérez-Prado M, Segurado J, Bohlen J, Gutiérrez-Urrutia I, Llorca J et al (2014) Measuring the critical resolved shear stresses in mg alloys by instrumented nanoindentation. Acta Mater 71:283–292
26. Loto RT, Babalola P (2017) Corrosion polarization behavior and microstructural analysis of AA1070 aluminium silicon carbide matrix composites in acid chloride concentrations. Cogent Engineering 4:1422229
27. Akinwamide SO, Abe BT, Akinribide OJ, Obadele BA, Olubambi PA (2020) Characterization of microstructure, mechanical properties and corrosion response of aluminium-based composites fabricated via casting—a review. Int J Adv Manuf Technol:1–17
28. Lin G, Zhang H-W, Li H-Z, Guan L-N, Huang L-J (2010) Effects of Mg content on microstructure and mechanical properties of SiCp/Al-Mg composites fabricated by semi-solid stirring technique. Trans Nonferrous Metals Soc China 20:1851–1855
29. Akinwamide SO, Akinribide OJ, Phumlani M, Ayodele OO, Mophoso KL, Abe BT et al (2020) Influence of heat treatment on microstructural and mechanical behavior of stir cast Al-(TiFe-SiC) composites. Proceedings, Materials Today
30. Urena A, Martınez E, Rodrigo P, Gil L (2004) Oxidation treatments for SiC particles used as reinforcement in aluminium matrix composites. Compos Sci Technol 64:1843–1854
31. Wang M, Zhao Y, Wang L-D, Zhu Y-P, Wang X-J, Sheng J, Yang ZY, Shi HL, Shi ZD, Fei WD (2018) Achieving high strength and ductility in graphene/magnesium composite via an in-situ reaction wetting process. Carbon 139:954–963
32. Albiter A, Contreras A, Bedolla E, Perez R (2003) Structural and chemical characterization of precipitates in Al-2024/TiC composites. Compos A: Appl Sci Manuf 34:17–24
33. Zhang Z, Chen D (2006) Consideration of Orowan strengthening effect in particulate-reinforced metal matrix nanocomposites: a model for predicting their yield strength. Scr Mater 54:1321–1326
34. Casati R, Vedani M (2014) Metal matrix composites reinforced by nano-particles—a review. Metals 4:65–83
35. Chen A-L, Arai Y, Tsuchida E (2005) An experimental study on effect of thermal cycling on monotonic and cyclic response of cast aluminium alloy-SiC particulate composites. Compos Part B 36: 319–330
36. Zimmerman A, Palumbo G, Aust K, Erb U (2002) Mechanical properties of nickel silicon carbide nanocomposites. Mater Sci Eng A 328:137–146
37. Reddy MP, Shakoor R, Parande G, Manakari V, Ubaid F, Mohamed A et al (2017) Enhanced performance of nano-sized SiC reinforced Al metal matrix nanocomposites synthesized through microwave sintering and hot extrusion techniques. Progress in Natural Science: Materials International 27:606–614
38. Swamy A, Ramesha A, Kumar GV, Prakash J (2011) Effect of particulate reinforcements on the mechanical properties of Al6061-WC and Al6061-gr MMCs. J Miner Mater Charact Eng 10:1141–1152
39. Guo J, Gougeon P, Chen X-G (2012) Study on laser welding of AA1100-16 vol.% B4C metal–matrix composites. Compos Part B 43:2400–2408
40. Pityana S, Fedotova T, Popoola O (2011) Quantitative study of the hardness property of laser surface alloyed aluminium AA1200. J South Afr Inst Min Metall 111:335–344
41. Mohapatra S, Chaubey AK, Mishra DK, Singh SK (2016) Fabrication of Al–TiC composites by hot consolidation technique: its microstructure and mechanical properties. Journal of Materials research and Technology 5:117–122
42. Pardo A, Merino M, Merino S, Viejo F, Carboneras M, Arrabal R (2005) Influence of reinforcement proportion and matrix composition on pitting corrosion behaviour of cast aluminium matrix composites (A3xx. x/SiCp). Corros Sci 47:1750–1764
43. Trowsdale A, Noble B, Harris S, Gibbins I, Thompson G, Wood G (1996) The influence of silicon carbide reinforcement on the pitting behaviour of aluminium. Corros Sci 38:177–191
44. Katkar V, Gunasekaran G, Rao A, Koli P (2011) Effect of the reinforced boron carbide particulate content of AA6061 alloy on formation of the passive film in seawater. Corros Sci 53:2700–2712
45. Mayyas AT, Hamasha MM, Alrashdan A, Hassan AM, Hayajneh MT (2012) Effect of copper and silicon carbide content on the corrosion resistance of Al-Mg alloys in acidic and alkaline solutions. J Miner Mater Charact Eng 11:335–352
46. Loto RT, Babalola P (2018) Effect of alumina nano-particle size and weight content on the corrosion resistance of AA1070 aluminum in chloride/sulphate solution. Results in Physics 10:731–737
47. Gupta R, Sukiman N, Cavanaugh M, Hinton B, Hutchinson C, Birbilis N (2012) Metastable pitting characteristics of aluminium alloys measured using current transients during potentiostatic polarisation. Electrochim Acta 66:245–254
48. Rivai AK, Takahashi M (2008) Compatibility of surface-coated steels, refractory metals and ceramics to high temperature lead–bismuth eutectic. Prog Nucl Energy 50:560–566
49. Han Y-M, Chen X (2015) Electrochemical behavior of Al-B4C metal matrix composites in NaCl solution. Materials 8:6455–6470
50. Sweitzer J, Shiflet G, Scully JR (2003) Localized corrosion of Al90Fe5Gd5 and Al87Ni8. 7Y4. 3 alloys in the amorphous, nanocrystalline and crystalline states: resistance to micrometer-scale pit formation. Electrochim Acta 48:1223–1234
51. Liu Z, Wu B, Gu M (2007) Effect of hydrolysis of AlN particulates on corrosion behavior of Al/AlNp composite in neutral chloride solution. Compos A: Appl Sci Manuf 38:94–99
52. Reboul M, Baroux B (2011) Metallurgical aspects of corrosion resistance of aluminium alloys. Mater Corros 62:215–233
53. Akinwamide SO, Lemika SM, Adams F, Akinribide OJ, Abe BT, Olubambi PA (2019) An investigation on the corrosion behavior of Al (mg-TiFe-SiC) matrix composite in acidic and chloride media. Materials Today: Proceedings 18:3827–3834
54. Zakaria H (2014) Microstructural and corrosion behavior of Al/SiC metal matrix composites. Ain Shams Engineering Journal 5:831–838
55. Lindroos V, Talvitie M (1995) Recent advances in metal matrix composites. J Mater Process Technol 53:273–284
56. Muley AV, Aravindan S, Singh I (2015) Nano and hybrid aluminum based metal matrix composites: an overview. Manufacturing Review 2:15